Seismic Structure Beneath Zagros-Makran Transition Zone (Iran) from Teleseismic Study: Seismological Evidence for Underthrusting and Buckling of the Arabian Plate Beneath Central Iran

Farzam Yamini-Fard[1] and Denis Hatzfeld[2]

1. Assistant Professor, Seismology Research Center, International Institute of Earthquake Engineering and Seismology, Tehran, Iran, email: faryam@iiees.ac.ir
2. DR1 CNRS, Laboratoire de Géophysique Interne et Tectonophysique, Joseph Fourier University, Grenoble, France

ABSTRACT: *Receiver function analysis in transition zone between the Zagros collision zone and the Makran subduction zone shows gradual increment of the Moho depth to ~58km into the north. The Moho depth is ~32km beneath western end of the Makran prism (58º E-26.6ºN). Furthermore, crust thickening to ~58km is observed 60km west of the Zendan-Minab-Palami fault system (ZMP) that is unusual for this part of the Zagros. This implies deflection of the Arabian Platform west of the ZMP. The Moho upwarp under region of the Khurgu indicates that the mountain ranges were lifted enmasse as a result of crustal buckling under horizontal compression. Moho depth variation beneath other stations in eastern end of the Zagros is around ~45km and increases into north to ~53km beneath Main Zagros Thrust (MZT). Strong PS conversion is observed under Zendan-Minab-Palami fault system in upper crust that could be related to unconsolidated material associated with this fault. Inversion of P travel time residuals suggests a low velocity zone beneath the transition zone in accordance with the receiver function result. This information implies underthrusthing of the Arabian plate beneath the Central Iran and the gradual transition into thinner crust beneath the accretionary prism of the Makran.*

Keywords: Seismic structure; Receiver function; Teleseismic tomography; Zagros; Makran; Iran

1. Introduction

The deep structure of the Zagros-Makran transition zone is poorly known. The Bouguer anomaly map shows a negative anomaly near the *MZT* and an important gradient in transition zone, see Figure (1) [3]. This gradient probably associated with transition from thick sediments of Zagros into Ophiolite series of Makran [17]. Dehghani and Makris [3] estimate the crust thickness of 55*km* beneath *MZT*, 40*km* beneath Lut desert and 25*km* along the Makran coast. They suggest that large variation between (-70 to 70*mgal*) in transition zone can be due to contrast between oceanic lithosphere related to sediments of the Makran prism and the continental lithosphere beneath the Zagros.

Niazi et al [14] using three explosions recorded in the Oman Gulf, south-west of the Jask region by *OBS* stations, estimate a 20*km* thick oceanic crust including 12*km* thick sedimentary layer above 6.7*km* thick volcanic layer. They estimate a 3º dip instead of 1º dip suggested by White and Klitgord [19] for the subducted slab in the western Makran coast. Kopp et al [11], using seismic profiles in the region limited between 23.5º-25º*N* and 62º-63.5º*E* suggest an average of 3º dip slab with a zone décollement in

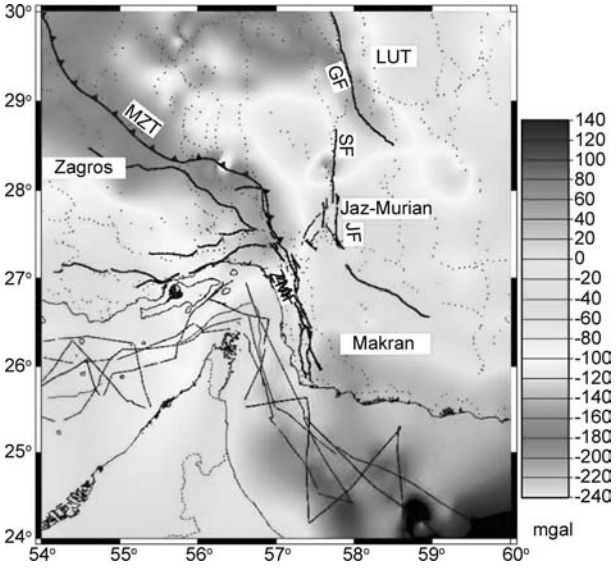

Figure 1. Bouguer gravity anomaly and important faults in transition zone and its neighborhood. We can observe large gradient in transition of Zagros-Makran. Data is obtained from BGI (Bureau of Gravimetric International). The gravimetric stations are shown by dots. JF (Jiroft Fault), SF (Sabzevarn Fault), ZMP (Zendan-Minab-Palami fault system), MZT (Main Zagros Thrust), and GF (Gowk Fault).

8.5*km* depth. They estimated a 9*km* thick oceanic crust in south of deformation front, and 7*km* thick sediments that injected on that.

Paul et al [15] find evidence of crust thickening in the Zagros mountain range resulted from crustal-scale thrusting by analysis of receiver functions calculated from 45 temporary seismological stations and gravity modelling. They conclude that Moho is almost horizontal with a little variation around 45*km* from coast of Persian Gulf to 25*km* southwest of the Main Zagros Thrust (*MZT*). Migration of receiver functions also shows an abrupt increase of crust thickness to ~70*km* beneath Sanandaj-Sirjan metamorphic zone that is between 50 and 90*km* northeast of the surface exposure of the *MZT* on 53°*E*. Further northeast, beneath Urmieh-Dokhtar magmatic assemblage and the southern part of the Central Iranian micro-continent, the Moho depth decreases to ~42*km*. They emphasized that thickest crust is located ~75*km* to the northeast of the Bouguer anomaly low at -220*gals*. Yamini-Fard et al [22] find other evidence of crust thickening to 60*km* inferred from receiver functions beneath *MZT* in 51°*E* and even 60*km* southeast of the surface exposure of the *MZT*, that is greater than 48*km* obtained for the central Zagros [5] but is close to the value obtained by Paul et al [15] beneath and northeast of the *MZT*.

Ravaut et al [16] interpret the large-scale gravity low over Zagros-Oman mountains and foreland in terms of elastic flexure of the Arabian lithosphere. They explain this deflection by different loads, including topography, ophiolite nappes, sedimentary fill and the accretionary prism of the Makran trench. Modelling 2*D* deflection of the Arabian plate show that remnant ophiolites are isolated from Tethyan oceanic lithosphere in the Gulf of the Oman by a continental basement ridge, a *NW* prolongation of the Saih-Hatat window. Loading the northward-limited ophiolite blocks explains the deflection of the Fiqa foredeep basin. They relate the Tertiary Pabdeh foredeep to the emplacement of a 8-km-thick tectonic prism located on the Musandam Peninsula and in the Hormuz strait. They discuss evolution of the northern Oman margin in the framework of Late Cretaceous obduction of the Tethys and synchronous subduction and exhumation of the Oman margin.

The deep structure of the Zagros-Makran transition zone has been studied by two-three months teleseismic data of the Minab and Khurgu profiles. In fact the transition is from the Zagros continental collision zone with thick sediments to the Makran oceanic subduction including the thick prism and Ophiolites.

2. Minab Seismic Profile

25 Minititan stations, three components with continuous recording and 125*Hz* sampling frequency, were installed on a 300*km* long profile, see Figure (2). They included 7 *CMG*40 (20*s*) broad-band, 11 Lennartz *Le*3*D* (5*s*) medium-band and 7 *L*22 (1*s*) short-period seismometers. The goal was to find the difference between the structure beneath eastern end of the Zagros and western end of the Makran. The distance between stations was selected between 10-15*km*. Available roads affected the direction and location of profile.

3. Teleseismic Tomography

3.1. Data

Totally 53 teleseismics with $mb \geq 5$ were recorded by minimum 10 stations in epicentral distance between 25° and 95°. Azimutal distribution of 50 teleseismics is between 25° and 95° and 3 between 220° and 300°, see Figure (3). Therefore, a majority of teleseismics were located in Pacific belt. Teleseismics were extracted from continuous data after time correction. Minab profile included 3 different seismometers.

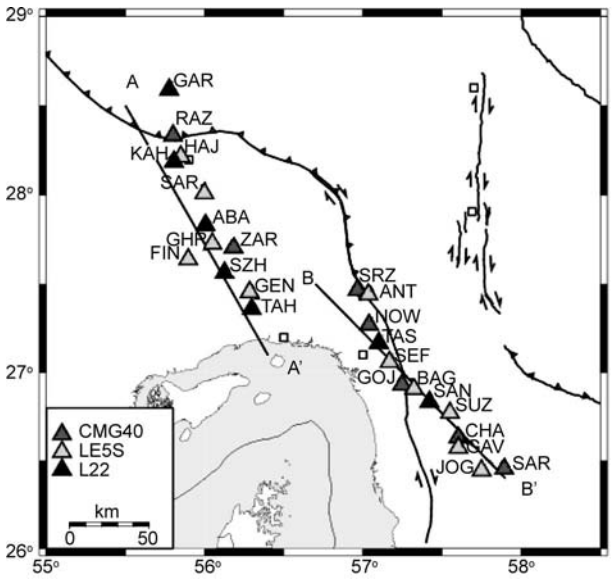

Figure 2. Minab temporary seismic profile installed from November 17, 1999 to January 6, 2000 in Zagros-Makran transition zone. Seismometers are L22 (short-period), Le5s (medium-band) and CMG40 (broad-band).

After instrument correction each record was convolved by a 4^{th} order band pass Butterworth filter between 0.5 and 2*Hz*. The first arrival at a good station was selected as the reference, then the first arrivals in other stations were picked using cross correlation operator. Finally the result of cross correlation was checked visually. To have much precision, the first clear maximum or minimum observed on all seismograms was picked. In total 855 *P* phase arrival times were obtained.

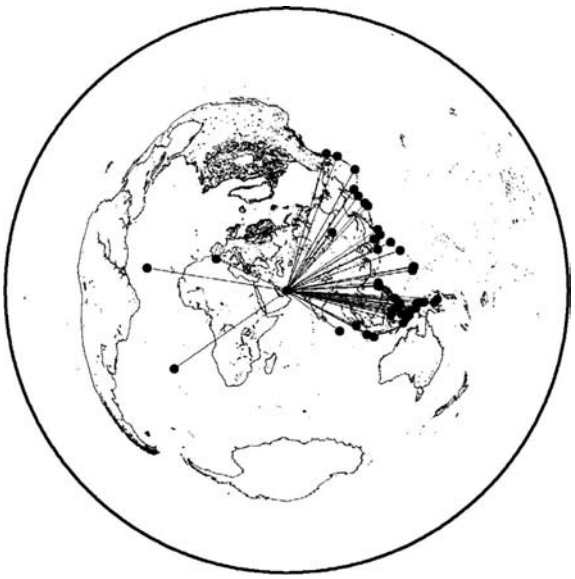

Figure 3. Location of teleseismics recorded in Minab experiment to study seismic velocity anomalies by ACH tomography method.

Residuals are calculated using the *NEIC* bulletin (National Earthquake Information Centre) locations and *IASP*91 model [10]. Variation of residuals with azimuth was checked for each station to find possible abnormal residuals. The similarity of variations for near stations verifies the coherency of the result and quality of the data [21].

To decrease the residuals that could have the source except for velocity anomalies, like location error and selected reference model, we studied relative residuals. It is subtraction of station residual from reference residual. Two types of references were examined: average of residuals for each event and the residual of the reference station. The reference station recorded the majority of events and supposed to be located on a relatively homogenous structure. Figure (4) shows static terms obtained by two methods. This term is the average of relative residual for all events recorded at each station. The stations are projected on the line in $N40^{o}W$ direction, see Figure (5). ~1 second jump is observed for the stations close to the surface exposure of the Zendan-Minab-Palami fault system.

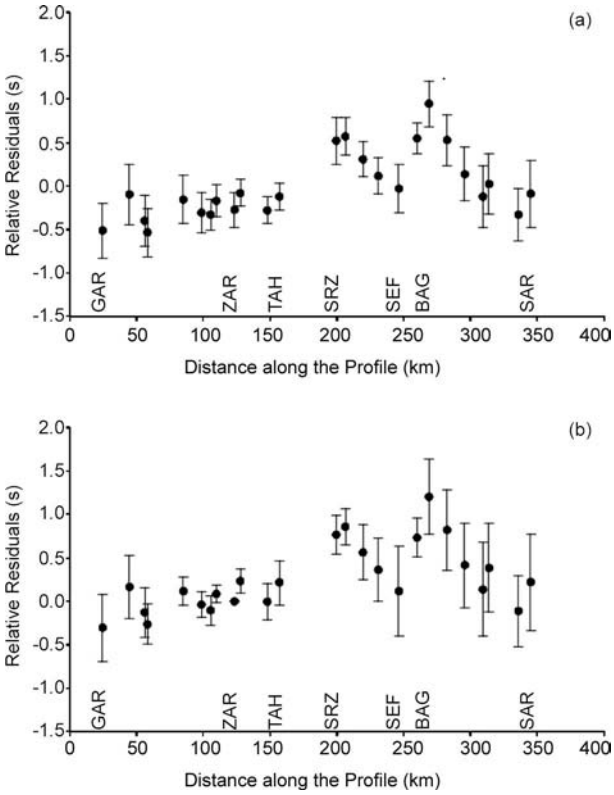

Figure 4. Average of the relative residuals for each station in function of distance on profile: a) reference is average of residuals for all stations that recorded each event (53 teleseismics); b) reference is the relative residual calculated for the ZAR station for each event (48 teleseismics). Averages are presented with their standard deviation.

Figure (5) shows variation of the relative residuals in function of the azimuth (epicentral region). The events are grouped in 20 degrees back-azimuth slices. The curves show good coherency in amplitude and their variation in function of the back-azimuth that verifies good quality of the data. Remarkable variation of relative residuals is observed for the stations located near *ZMP*. Important anomaly affects the rays coming from 40° to 80°. For all azimuth slices, 2 picks are observed near *BAG*, *GOJ*, *SRZ* and *ANT* stations located close to *ZMP*. In opposite, big variations for the stations situated on Zagros were not observed.

3.2. Inversion of Relative Residuals

The *ACH* method was applied for inversion of the observed *P* time residuals [1, 6]. Inversion program box written by Judenherc [8] was used for teleseismic tomography.

Different initial models were tested and perturbations in each block of the resulted model were examined. To minimize the inversion parameters 4 layers model was selected. We consider thickness of our model 190*km*, 2/3 of length of profile. Considering the geometry of the rays near free surface one cone is considered beneath each station [6]. This geometry permits to concentrate effect of heterogeneous superficial structures inside of cone as the first layer. To decrease the effect of dimension of selected boundaries, 8 inversions for each layer were done. The center of the blocks is shifted 1/3 and 2/3 length of each block in north-south and east-west directions. Then the average of the results from 9 inversions was

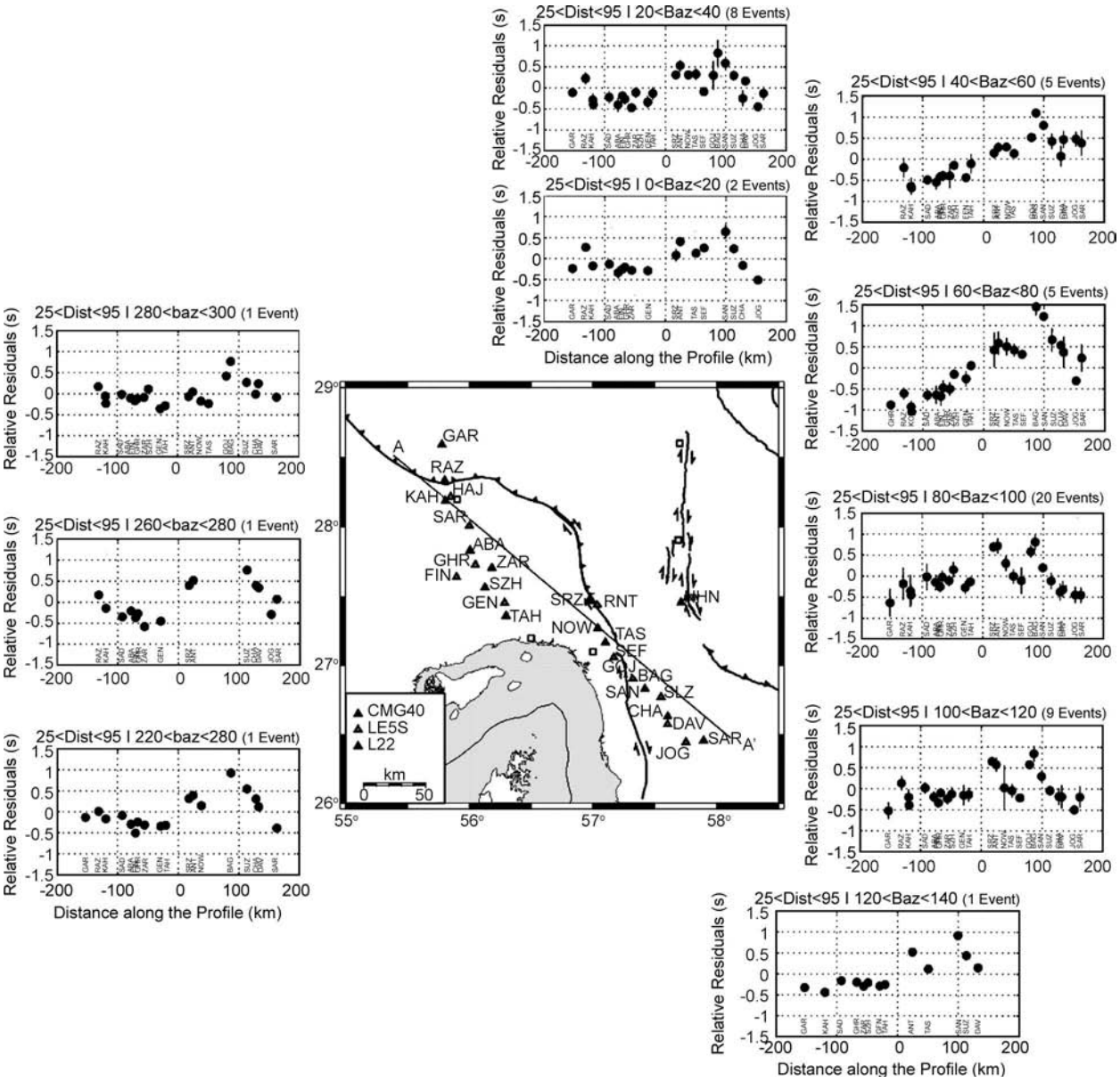

Figure 5. Relative residual curves for rays coming from different epicentral regions.

calculated as the final result.

Table (1) shows the initial model selected for inversion that is located in center on 27.5° *N*- 57.25° *E*. If 5 or more rays passed from each block it was considered in inversion. Different damping factors were tested and 80 were selected, see Figure (6). Selecting other values also did not change the result.

Table 1. Initial model used for inversion of the P teleseismic residuals.

Layer Number	Thickness (km)	Block Dimensions (km×km)
0	10	Cones
1	40	30×30
2	60	40×40
3	80	50×50

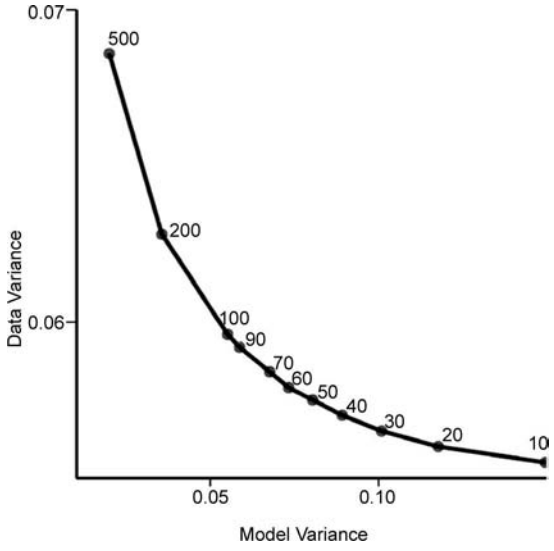

Figure 6. Effect of the damping factor on coupling of data variance and model variance. Damping factors are shown above each point.

Reduction of residual variance after inversion is 75%, see Figure (7). Diagonal value of the resolution matrix is 85% for most of the studied region that is in suitable range and standard error is 0.3. Different initial models were tested changing its geometry but the result did not differ much [21]. For example increasing the number of layers only decreased the resolution but did not change the result. Also the result is independent of layer velocities in the initial model. Testing different models with different total thicknesses shows that the value of perturbation is function of model thickness. However, it is clear that a majority of the anomalies is situated in the crust.

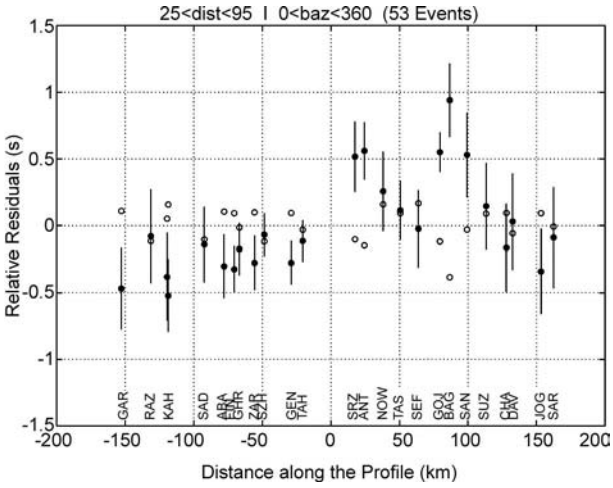

Figure 7. Average of residuals for each station before (black circles) and after (hollow circles) inversion.

3.3. Result of Teleseismic Tomography

Calculated perturbations relative to initial model, see Table (1), are presented in Figures (8) and (9) for each layer. The strong perturbation is observed in first layer of the model under *SRZ*, *ANT*, *BAG*, *GOJ* and *SAN* stations. Two slow zones in 10 to 50*km* layer could be correlated with the trace of the Zendan-Minab-Palami fault system on surface. Profile passed two times very close to the exposure of the *ZMP* and each time negative anomalies appeared beneath stations near fault zone which suggests a superficial anomaly. Another slow anomaly in crust but associated with less perturbation is observed near the Main-Zagros-Thrust. For deeper layers in upper mantle, a transition from slow zone to rapid zone was observed. A rapid zone appears in eastern end of profile beneath the accretionary prism of the Makran.

4. Receiver Function Analysis

4.1. Calculation

To study the receiver functions, the teleseismics with epicentral distance between 25° and 95° and magnitudes greater than 5 were selected. To calculate receiver functions the iterative deconvolution in time domain was applied as following [12]:

a) Calculation of the radial and transverse components;

b) Filtering with 4^{th} order Butterworth band-pass filter, 0.05-0.8*Hz*. The frequency range was selected considering the microseismic noise near the Gulf of Oman;

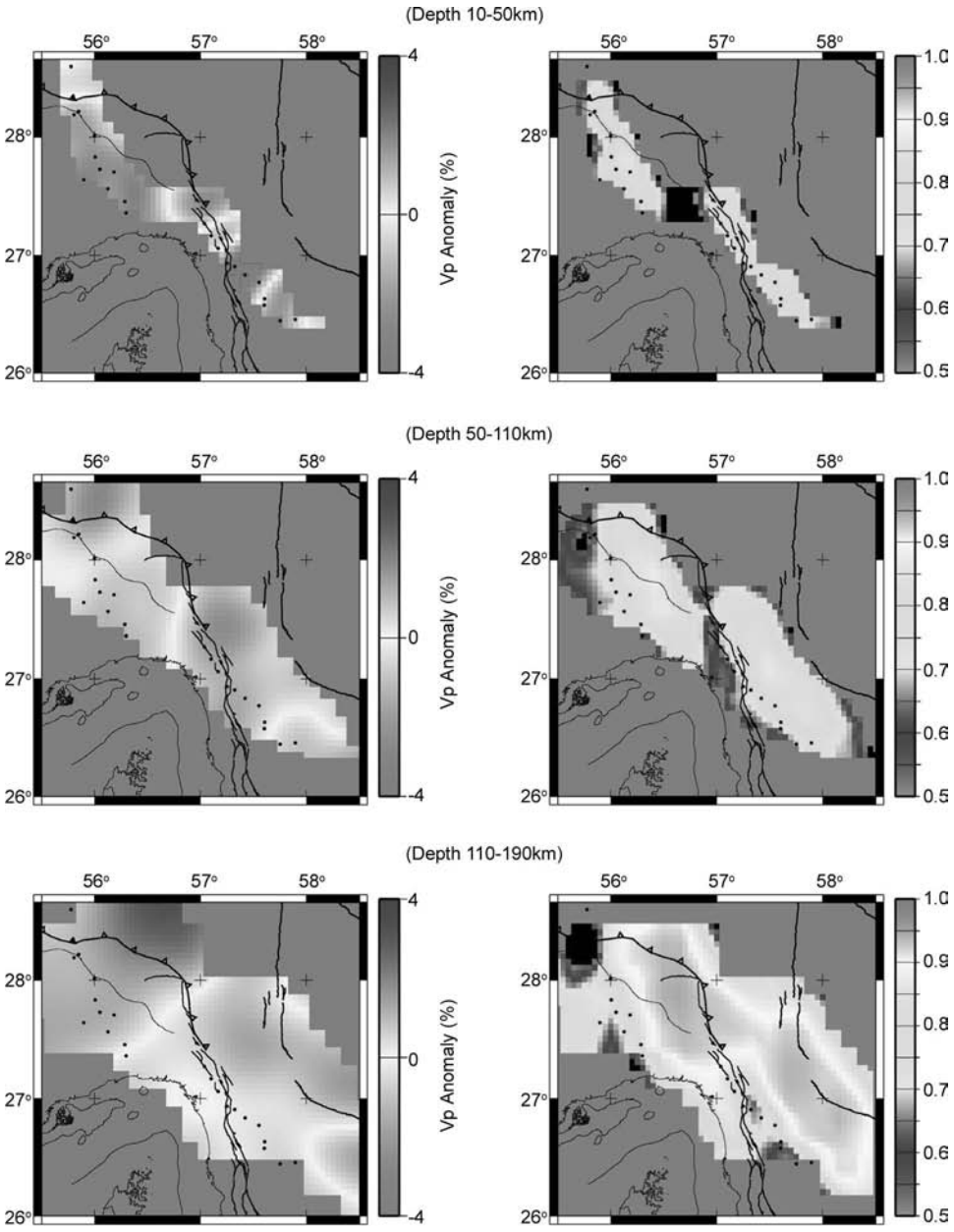

Figure 8. Topographic images for three layers: 10-50km, 50-110km and 110-190km. Right figures show the diagonal value of resolution matrix for each layer.

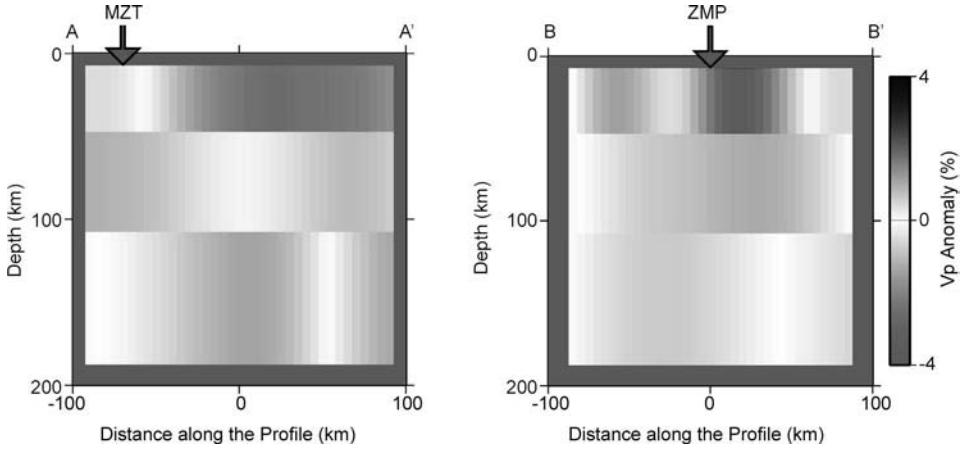

Figure 9. Depth profile velocity models. Principle faults are shown above the profiles: MZT (Main-Zagros-Thrust) and ZMP (Zendan-Minab-Palami) fault systems.

c) Extracting 10 seconds before and 50 seconds after first *P* wave arrival to see conversions from Moho and multiples;
d) Calculation of receiver functions by iterative deconvolution in time domain.

To calculate receiver functions the intercorrelation between *Z* component and radial component is determined. The result is normalised by the maximum autocorrelation of *Z* component. Time of maximum intercorrelation and its value are added to receiver function as a Dirac. The result is subtracted from radial component. Then the steps were repeated 30 times and the receiver function was convolved with a Gaussian with 0.3 second width. This number permitted us to see a majority of signals in radial component.

4.2. Data Selection Criteria

Theoretically maximum amplitude of the receiver function must be on the beginning of the signal. But *PS* conversions from sedimentary basin interface can create the waves with larger amplitude after *P* direct wave. Besides, only some interfaces can generate *PS* conversion wave, so ideally the receiver function must be simple. The traces were selected with a good signal to noise ratio that could decrease the maximum amplitude of the intercorrelation between *Z* and radial components. Noise can create numerous large amplitudes on receiver functions.

If the interface in the isotropic medium is considered horizontal the *SH* wave is not generated from *P* incidence. However, even when the signal to noise ratio is high, three phenomenons can explain high energy in transverse component: diffraction, dipping interface and anisotropy.

Considering above mention criteria totally 54 receiver functions were selected for analysis, see Table (2).

4.3. Receiver Function Analysis

Generally, receiver functions beneath two profiles are not simple. Low number of selected ones during 2 months record could have two reasons: 1) quality of data and 2) complex structure beneath stations [21], see Table (2). To find the reason we calculated receiver functions by two years data that were recorded by *BNDS* station. *BNDS* is one of the permanent stations which belongs to Iranian Broadband National Seismic Network located above Geno mountain very close to the *GEN* station. Again calculated receiver functions are not simple and good coherency can be seen between the stacked receiver functions for *GEN* and *BNDS* stations, see Figure (10). Therefore, it is more logic to accept

Table 2. Number of selected receiver functions for each station.

ANT	CHA	DAV	GEN	GHR	HAJ	GOJ	NOW	RAZ	SAR	SRZ	SUZ	ZAR
7	3	5	5	2	2	4	7	2	4	3	8	2

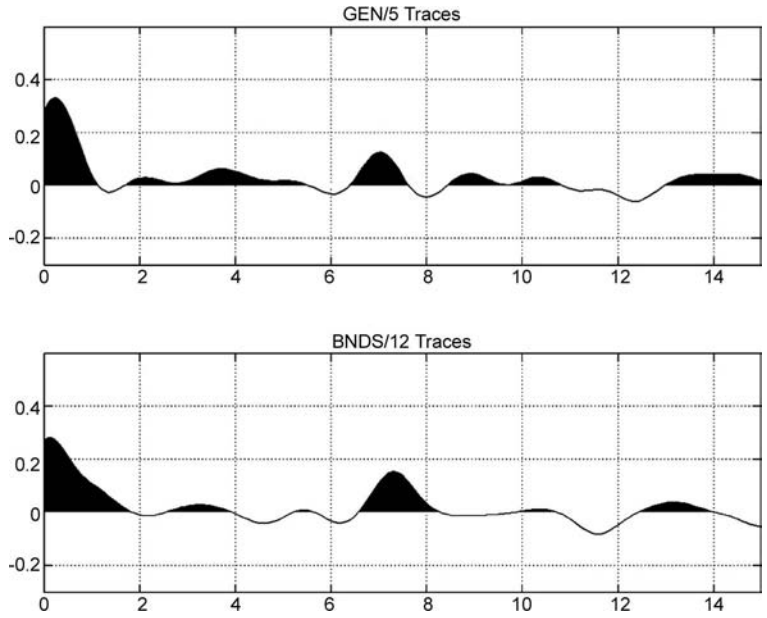

Figure 10. Stacking of calculated receiver functions for GEN and BNDS stations very close to each other.

existence of the complex structure under stations than bad quality of data. Examining transverse receiver functions, noticeable energy was also found on data [21]. To study diffraction, dipping and anisotropy effects on receiver functions, more data was needed with good azimuthal coverage.

Stacking receiver functions for each station show good coherency between them from each station to other close station. It could be a good control where the number of data is low like our case, see Figures

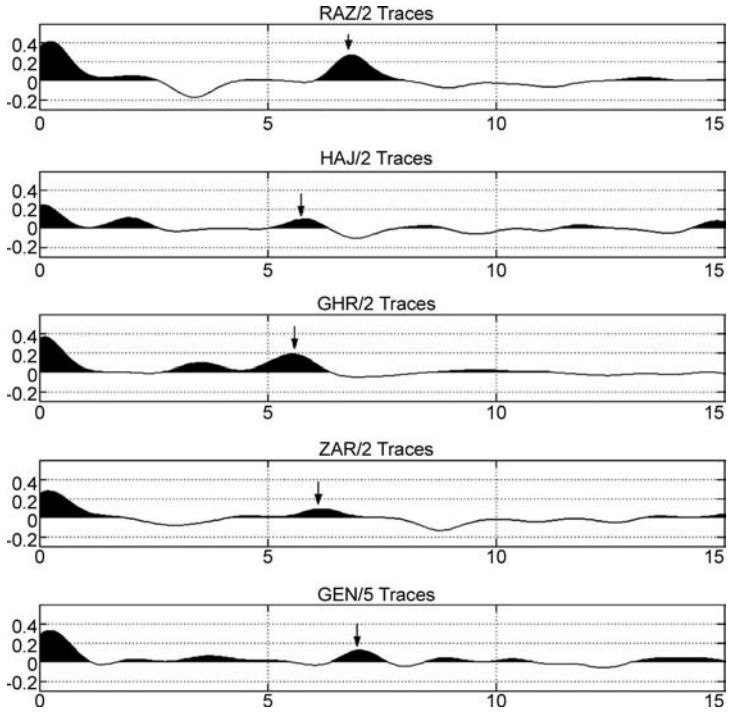

Figure 11. Stacked receiver functions for the stations located in eastern end of the Zagros.

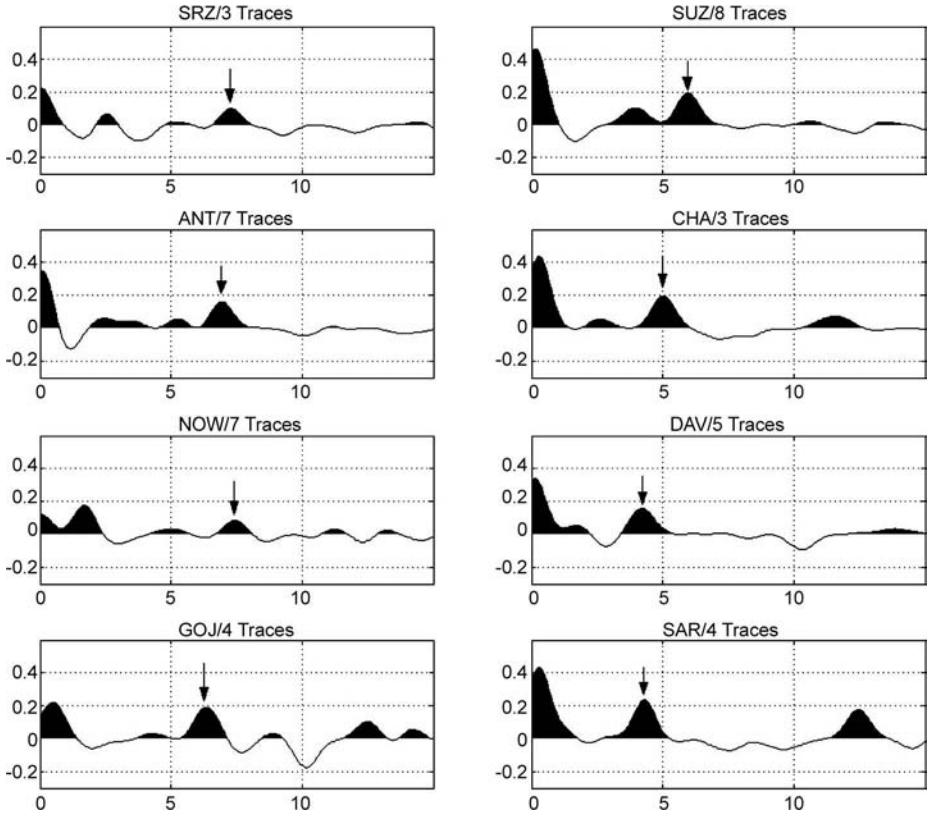

Figure 12. Stacked receiver functions for stations located in western end of the Makran and close to ZMP.

(11) and (12). A move-out correction has been done before stacking to a constant slowness of 7*s/deg* using *IASPEI* model with *vp/vs*, 1.76 [23].

For stations on the Zagros we can see conversions for *GEN* and *RAZ* at ~7 seconds and for *ZAR*, *HAJ* and *GHR* stations at ~5.5-6 seconds, see Figure (11). ~4-5 seconds *PS* conversion is seen beneath *SAR*, *DAV*, *CHA* and *SUZ* stations that are located near the prism of Makran, see Figure (12). There is other pick on ~6 seconds with larger amplitude for *SUZ* station. Strong conversion was observed between ~6-7 seconds beneath *SRZ*, *ANT*, *NOW*, *GOJ* very close to Zendan-Minab-Palami fault system. We can see other conversion at less than ~3 seconds that is characteristic of these stations. For example, for *NOW* station, the first arrival has low amplitude and the largest pick on receiver functions is located 2 seconds after. In other example for first arrival, the *GOJ* station is shifted to right.

4.4. Migration of Receiver Functions

The position of probable interfaces was calculated in depth using Common Conversion Point method [24]. To migrate receiver functions, *vp/vs* ratio 1.76 was selected [5, 23]. The volume under profile is binned to three directions. The amplitudes of radial receiver functions with ray paths crossing the bin averaged as the amplitude of each bin. In this study the dimension of cellules was selected 2*km* horizontally and 5*km* vertically. Finally, we smoothed the result by a 2 dimensional Gaussian in horizontal direction. Images obtained by *CCP* migration reflect important crustal thickness variation beneath profile that will be discussed later, see Figure (13).

One interface in ~32*km* was observed beneath *SAR* and *DAV* stations were located in eastern end of Minab profile on the Makran. Towards north, we observed increment of the Moho depth to ~45 beneath *SUZ*, ~50*km* beneath *GOJ* and finally to ~58*km* beneath *NOW*, *ANT* and *SRZ* stations. Other interface is observed at ~32*km* Beneath *SUZ* station as for *SAR* and *DAV* stations. An interface in upper crust creates high amplitude *PS* conversions beneath *ZMP*.

For the Zagros profile one interface observed beneath *GEN* station with ~59*km* depth. Into north, the depth decrease to 45*km* beneath *ZAR*, *GHR* and *HAJ* stations with a jump, then in other jump increase to ~53*km* beneath *RAZ* station very close to trace of the *MZT*.

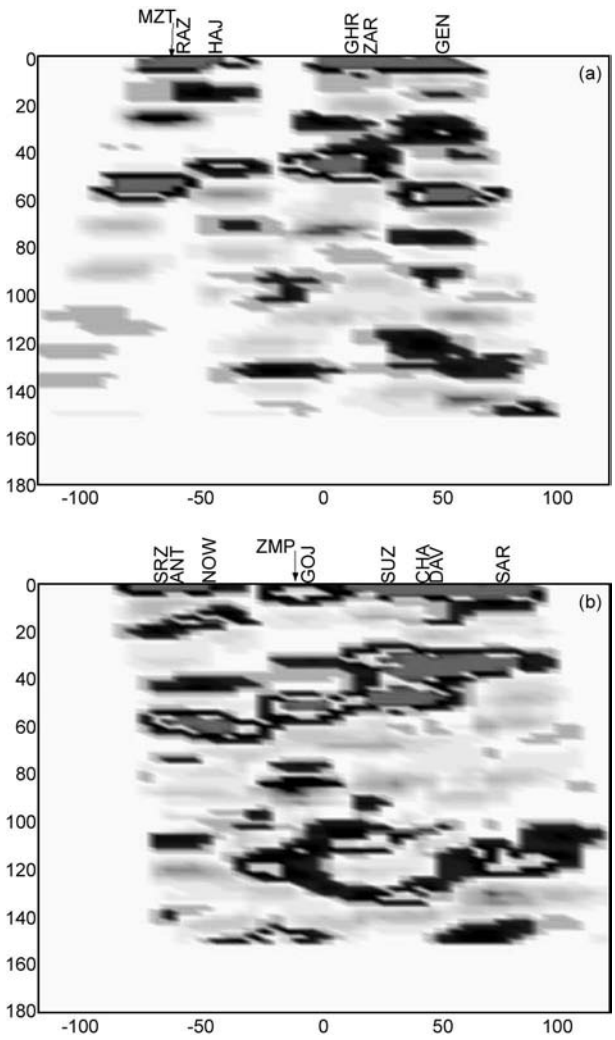

Figure 13. Depth profiles beneath eastern end of the Zagros (a) and western end of the Makran (b) obtained by migration of receiver functions. Scale of the colors is in function of average of converted wave amplitudes relative to P ampiltude in each interface.

4.5. Khurgu Seismic Profile

In another field study, we deployed 31 stations to study microseismicity of the Khurgu region from March 1, 2006 to June 15, 2006, see Figure (14). The instruments were *CMG*-6*TD* (10*s*), and data was recorded continuously with sampling frequency 100*Hz*. During this recording time 41 teleseismics with $mb \geq 5.5$ were recorded in epicentral distance between 25° and 95°. Following the same procedure as described for profile of the Minab, 163 were selected between 1332 calculated receiver functions, see Table (3).

To have some idea about probable changes in depth of the Moho. We examined receiver functions along the *N*40°*E* profile. Figure (15) shows stacked receiver functions for each station. Considering receiver functions from *SW* to *NE* for *BNDS* and

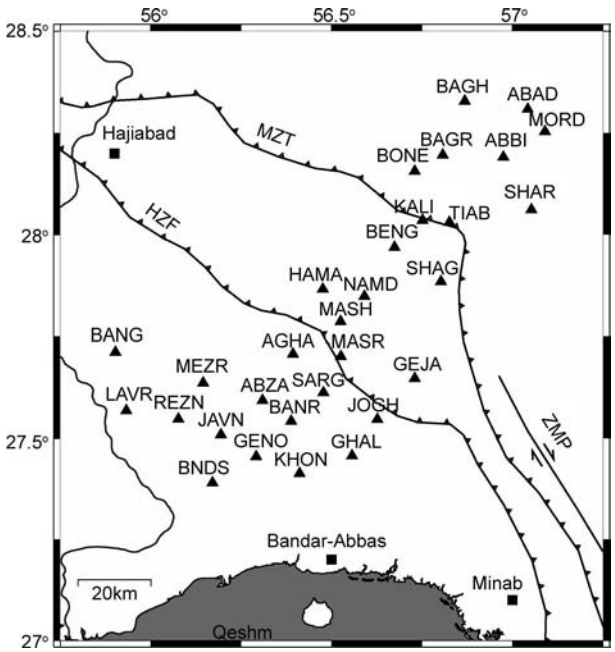

Figure 14. Temporary seismic network installed from March 1, 2006 to June 15, 2006 in Khurgu region.

Table 3. Number of selected receiver functions for each station on Khurgu profile.

ABAD	ABBI	ABZA	BNDS	GENO	MORD	NAMD	MASR	SARG	SHAG	SHAR	TIAB
5	7	15	15	8	9	26	22	17	22	7	10

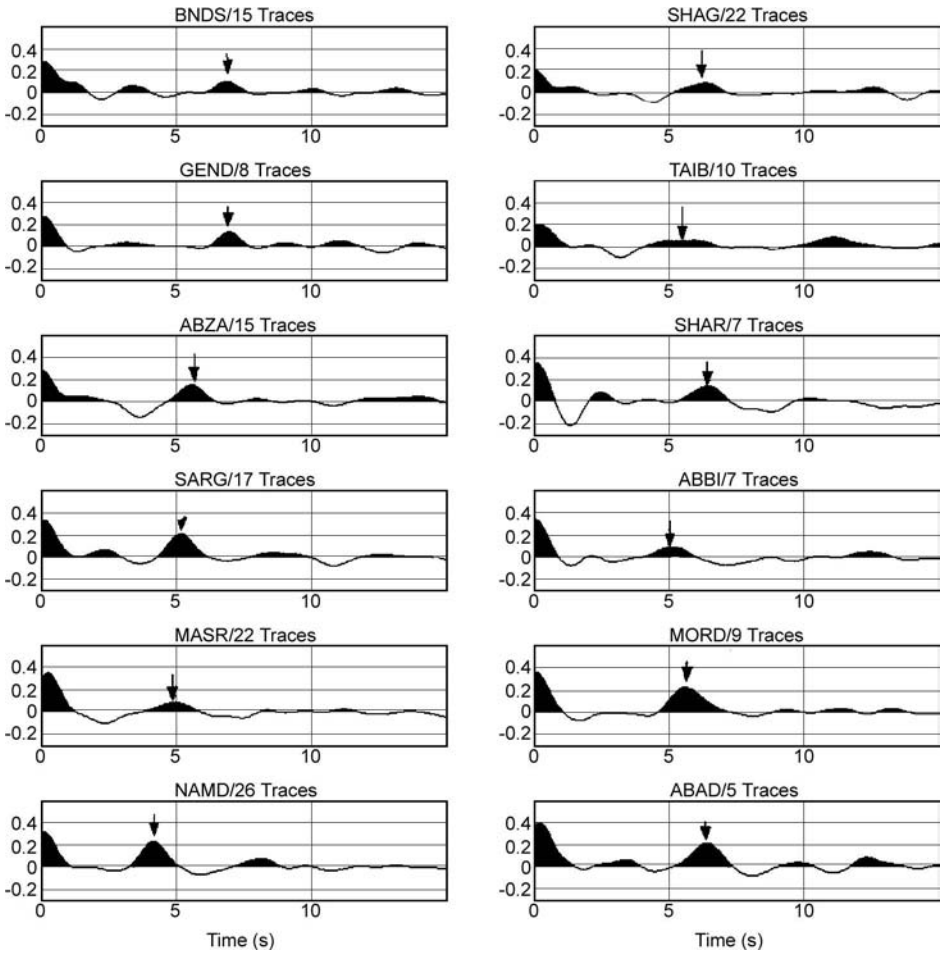

Figure 15. Stacked receiver functions for stations located in the Khurgu region.

GENO stations, a pick could be seen at ~7 seconds. Then the pick time decrease gradually to minimum ~4 seconds beneath *ABZA*, *SARG*, *MASR* and *NAMD* stations. For the rest of the stations we can see conversions at ~5.5-6.5 seconds.

The migration of selected receiver functions, assuming constant value of the velocities beneath stations, shows changes in Moho depth clearer, see Figure (16). Moho depth decrease gradually beneath High Zagros and again increase into *NE*, north of the *MZT*. Deeper Moho beneath *BNDS* and *GENO* stations is observed.

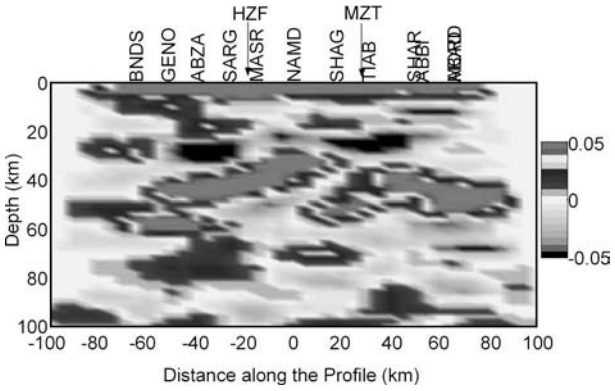

Figure 16. Migration of receiver functions beneath the profile of Khurgu oriented N40ºE. Scale of the colors is in function of average of converted wave amplitudes relative to P amplitude in each interface.

5. Discussion

This study shows an important variation of the structure across the Zendan-Minab-Palami fault system. Receiver functions beneath *SAR* and *DAV*, *CHA* stations close to the prism of Makran is relatively simple. We could follow a ~4-5 seconds conversion beneath these stations. This could be associated to a Moho located less than 40*km*. It is the first evidence of a thinner crust in eastern end of the Makran. This pick was seen also little more into north under *SUZ* station. It has less amplitude relative to other pick on 6 seconds. Tomography images also showed a rapid zone beneath these stations. The amount of perturbation is close to what was calculated beneath stations located in Zagrso.

Further into north from *CHA* to *SRZ* station, nearly parallel to *ZMP*, shifting of the pick was observed from ~5 to ~7 seconds. It could be related to gradual increment of the Moho depth into north. Therefore, it could be another evidence of underthrusting of the Arabian shelf beneath Central Iran. It implies a progressive transition between the Zagros continental zone and the Makran oceanic subduction [23]. Therefore, some of the observed low velocity in the tomography image could be related to deflection of the heterogeneous Arabian plate. Generally different reasons could be related to low velocity zones such as: a thick crust; existence of important fracture zone near major faults; existence of an unconsolidated sedimentary layer; high temperature zone, and change in composition of material.

Large amplitude conversions beneath stations close to Zendan-Minab-Palami fault system at less than 3 seconds (~15-20*km* depth) verify the existence of unconsolidated layer or a fractured zone and probably is associated with this fault system or a zone of décollement which creates strong impedance variation in upper crust. This is consistent with an observed low velocity zone beneath stations very close to *ZMP* calculated by 3-*D* inversion of teleseismic *P* wave residuals. 3-*D* inversion of the local data somehow shows low velocity zone in upper crust north-east of the *ZMP* beneath the Bashagard sedimentary basin [23]. Furthermore flysch zone is observed close to Zendan and Palami faults that is composed of unconsolidated sediments [13].

Therefore the receiver function analysis and the tomography images proved the possibility of the crustal thickening and presence of unconsolidated material in the upper crust. It is reason for ~1 second observed delay in *P* wave arrival time in transition zone. The resolution of data did not permit us to find other reasons for observed anomaly and to separate its origins individually.

Selected receiver functions for stations in eastern end of the Zagros show a decrement and again an increment in position picks. Put aside the result for the *GEN* station, Moho depth variations from south into north, from ~45 to ~53*km*, is very close to the calculated values by Paul et al [15]. But the ~7 seconds pick beneath *GEN* or *BNDS* stations were located close to the Geno mountain ~60*km* west of *ZMP* trace and ~80*km* south of the *MZT* trace is surprising. It could be an evidence for thick crust, ~59*km* depth. Tomography image for 10-50*km* slice does not show anomaly beneath the *GEN* station. Slow anomaly was observed even to the west of the *ZMP* trace for deeper slices.

It could be another evidence of thick crust south of the *MZT*, like the situation on 51º longitude [22]. Receiver functions beneath the profile of the Khurgu shows more complex structure at west of the *ZMP*.

Beneath the Geno mountain Moho depth is deep and decrease gradually into north-east beneath High Zagrso to minimum depth ~30-35*km* after ~10*km* jump. More into north possible Moho interface disrupted or diminished near *MZT* and depth increases gently to ~45*km*. It suggests that there is a Moho upwarp beneath High Zagros and a vertical separation of the Moho by ~5*km* beneath *MZT*. The cause of the Moho offset can be related to the crustal movement across the fault. Strike-slip motion could juxtapose crustal blocks of different thicknesses. The offset also can be produced by crustal deformation from horizontal compression. In response to the convergence and the horizontal shortening, the crust may be either vertically streched and create Moho depression, or it may buckle upward. It could be an explanation for the Moho upwarp under High Zagros. Bouguer gravity anomaly does not reflect such changes in the Moho depth [3], see Figure (1).

Paul et al [15] found some evidence of thick crust, ~70*km*, by receiver function analysis north of the *MZT* on 53º longitude. It is different from our result in south-eastern end of the *MZT*, ~ 45*km*. Therefore, it seems that thickening in different parts of Zagros is not similar. It could be related to the mechanism of deformation in each segment; rotation of the plates; irregular shape of Arabian shelf, or the existence of ridge on Arabian shelf [9]. Equally, we can consider possible irregularities in the crustal Iranian block border as other reason. In our case, transition is between the collision domain and the subduction domain so it is more logical that associate thickening of crust is beneath *ZMP* to underthrusting of Arabian plate into north-east beneath central Iran.

Furthermore, azimuth of the faults and folds, and seismicity trend follow the coastal line in west and north of the Hormuz strait. *GPS* measurements also reveal radial compression around Hormuz strait [2]. Underthrusting of Arabian plate in transition zone can not explain such phenomena by itself. In western part of the strait, deformation is accommodated by pure reverse mechanism and in eastern part the mechanism of the deformation is partial partitioning between right-lateral strike-slip and shortening components [18, 23].

Two tectonic models are suggested by Kadinsky-Cade and Barazangi [9]: ridge on underthrusting Arabian shelf and underthrusting of Arabian shelf promontory beneath Central Iran. Bayer et al [2] suggest rotation of the velocities and compressional strain axis as the result of seamount subduction of Musandam promontory in accordance with sandbox experiment of Dominguez et al [4].

GPS measurements and frontal thrusts along the coastal line and northeast trending zone of earthquakes support ridge on underthrusting Arabian shelf. White and Rose [20] associated a large basement ridge detected on multichannel seismic reflection data and gravity profiles to subsurface continuation of the Musandam peninsula beneath strait of the Hormuz. They believed that collision and underthrusting of the Arabian plate beneath Iran on which this ridge lies has caused many of large earthquakes that have occurred in this region. Kadinsky-Cade and Barazangi [9] suggest that such a ridge could represent a structural manifestation of Cretaceous allochtonous rocks originally overthrusted into the Arabian continent from the east. In this case some left-lateral strike slip faulting was expected in western edge of ridge that is suggested by Hessami et al [7] or Dominuguez et al [4] that has not been supported by seismological evidences so far and could be due to the dominant aseismic slip such as one for the *ZMP*.

The second model, promontories on Arabian shelf result in earlier stage of collision, and is suggested to explain some features in this region. In this case we should expect some bending of *MZT* consistent with the radial feature around Hormuz strait. Also some radial compressional axis pattern were expected in this region. But the trend of faults and folds around Hormuz strait is very different from trend of *MZT* in north. Furthermore, this model can not explain thick crust beneath *BNDS* and *GEN* stations. Therefore, the first model describes the observed seismotectonic and structure in this region but the reason for the origin of probable ridge is still under debate.

Our data can not show clearly the geometry 3*D* deflection of the Arabian plate corner suggested by Ravaut et al [16] beneath the Musandam Peninsula and Hormuz strait. However, thick crust beneath *GEN* and *BNDS* stations ~60*km* west of *ZMP* trace support this model. To map more details in this region, an extended seismological network in 2 dimensions and long period of the record were suggested due to the complex structure in this region.

6. Conclusions

Teleseismic tomography confirms an important variation of structure across Zendan-Minab-Palami fault system from Zagros rapid zone to slow zone that affects crust and upper mantle. Maximum

perturbation is observed close to Zendan-Minab-Palami fault system in crust. Analysis of the receiver functions, consistent with 3-D inversion of teleseismic *P* arrival residuals suggests thickening across transition zone that is seismological evidence of the underthrusting of the Arabian plate into north-east beneath central Iran. Large amplitude converted waves and slow zone in upper crust beneath the *ZMP*. It could be related to the unconsolidated material associated to this fault system. Furthermore, the receiver functions show an interface less than ~40*km* depth in western end of the Makran. That is the evidence of thinner crust beneath the accretionary prism of the Makran. Receiver functions beneath Geno mountains reveal unexpected thick Moho in north of Hormuz strait. That implies the deflection of the Arabian plate at west of the *ZMP*. However uplifting of crustal blocks in Khurgu region adjacent and within fault zone is most likely the result of the convergence and slip partition associated with local geometric complexities along the fault zone. In this region different faults converge to each other and the convergence between Arabian plate and central Iran must be accommodated in narrower zone. It could result in higher rate of stress accumulation and uplifting of the crustal block accommodated by arching across its northern or/and southern margin beneath the Geno region. That is different from other part of the Zagros which the continental convergence in plates boundaries supposed to be reflected just by crust thickening.

Acknowledgments

This study was supported by *IIEES* (International Institute of Earthquake Engineering and Seismology), *INSU-CNRS* (Intérieur de la terre) and the French Ministère des affaires etrangères in the frame of a co-operative research program. The authors would like to thank M. Ghafory Ashtiany, former president of *IIEES* for his support. We thank A. Paul, J. Vergne, and A. Kaviani for preparing analysis tools. We thank the *IIEES* and *LGIT* teams for support, administrative and field work assistance including A.M. Farahbod, M. Masoudi, M. Zolfaghari, M. Chizari, M. Taghaboni, M. Ghasemi, K. Assatourians, M. Parvazeh and H.R. Heidary-Moghadar, B. Bettig, C. Voisin, J.M. Douchain and M. Vallée. This work would have not been possible without the help of the people of the Hormozgan province and especially the local governor of Minab and Hormozgan University.

References

1. Aki, K., Christoffersson, A., and Husebye, E.S. (1976). "Three-Dimensional Seismic Structure of the Lithosphere under Montana LASA", Bull. Seism. Soc. Am., **82**, 501-524.

2. Bayer, R., Chéry, J., Tatar, M., Vernant, P., Abbasi, M., Masson, F., Nilforoushan, F., Doerflinger, E., Regard, V., and Bellier, O. (2006). "Active Deformation in Zagros-Makran Transition Zone Inferred from GPS Measurements", *Geophysical Journal International*, **165**, 373-381.

3. Dehghani, G.A. and Makris, J. (1984). "The Gravity Field and Crustal Structure of Iran", N. Jb Geol. Palaont. Agh., **168**, 215-229.

4. Dominguez, S., Malavieille, J., and Lallemand, S.E. (2000). "Deformation of Accretionary Wedges in Response to Seamount Subduction: Insights from Sandbox Experiment", *Tectonics*, **19**, 182-196.

5. Hatzfeld, D., Tatar, M., Priestley, K., and Ghafory Ashtiany, M. (2003). "Seismological Constraints on the Crustal Structure Beneath the Zagros Mountain Belt (Iran)", *Geophys. J. Int.*, **155**, 1-8.

6. Evans, J.R. and Achauer, U. (1993). "Teleseismic Velocity Tomography Using ACH Method: Theory and Application to Continental-Scale Studies", In: Iye, H.M. and Hirahara, K. (eds), Seismic Tomography: Theory and Practice, Chapman and Hall, Londres.

7. Hessami, K., Koyi, H., and Talbot, C. (2001). "The Significance of the Strike-Slip Faulting in the Basement of the Zagros Fold and Thrust Belt", *J. Petrol. Geol.*, 5-28.

8. Judenherc, S. (2000). "Etude et Caractérisation Des Structures Hercyniennes á Partir de Donnés Sismologiques: Le Cas du Massif Armoricain, Thèse de Doctorat", Université Louis Pasteur, Strasbourg I.

9. Kadinsky-Cade, K. and Barazangi, M. (1982). "Seismotectonics of Southern Iran: The Oman Line", *Tectonics*, **5**, 389-412.

10. Kennett, B. and Engdahl, E. (1991). "Travel Time for Global Earthquake Location and Phase Identification", *Geophys. J. Int.*, **105**, 429-465.

11. Kopp, C., Fruehn, J., Flueh, E.R., Reichert, C., Kukowski, N., Bialas, J., and Klaesschen, D. (2000). "Structure of the Makran Subduction Zone from Wide-Angle and Reflection Seismic Data", *Tectonophysics*, **329**, 171-191.

12. Ligorria, J. and Ammon, C. (1999). "Iterative Deconvolution and Receiver Function Estimation", Bull. Seism. Soc. Am., **89**, 1395-1400.

13. McCall, G.J.H. (1985). "Explanatory Text of the Minab Quadrangle Map 1:250,000", Geol. Surv. of Iran, Geological Quadrangle No. J 13.

14. Niazi, M., Shimamura, H., and Matsu'ura, M. (1980). "Microearthquakes and Crustal Structure off the Makran Coast of Iran", Geophys. Res. Lett., **7**, 297-300.

15. Paul, A., Kaviani, K., Hatzfeld, D., Vergne, J., and Mokhtari, M. (2006). "Seismological Evidence for Crustal-Scale Thrusting in the Zagros Mountain Belt (Iran)", *Geophys. J. Int.*, **166**, 227-237.

16. Ravaut, P., Bayer, R., Hassani, R., Rousset D., and Al Yahya'ey, A. (1997). "Structure and Evolution of the Northern Oman Margin: Gravity and Seismic Constraints Over the Zagros-Makran-Oman Collision Zone", *Tectonophysics*, **279**, 253-280.

17. Regard, V. (2003). "Variation Temporelle Spatiale de la Transition Subduction-Collision: Tectonique de la Transition Zagros-Makran (Iran) et Modélisation Analogique", Thèse de Doctorat, Université d'Aix-Marseille III.

18. Talebian, M. and Jackson, J. (2004). "A Reappraisal of Earthquake Focal Mechanisms and Active Shortening in the Zagros Mountains of Iran", *Geophys. J. Int.*, **156**, 506-526.

19. White, R.S. and Klitgord, K. (1976). "Sediment Deformation and Plate Tectonics in the Gulf of Oman", Earth Planet. Sci. Lett., **32**, 199-209.

20. White, R.S. and Ross, D.A. (1979). "Tectonics of the Western Gulf of Oman", *J. Geophys. Res.*, **84**, 3479-3489.

21. Yamini-Fard , F. (2003). "Sismotectonique et Structure Lithosphérique de Deux Zone de Transition Dans le Zagros (Iran): La Zone de Minab et la Zone de Qatar-Kazerun", Ph.D. Thesis, Joseph Fourier University, Grenoble I.

22. Yamini-Fard, F., Hatzfeld, D., Tatar, M., and Mokhtari, M. (2006). "Microearthquake Seismicity at the Intersection between the Kazerun Fault and the Main Recent Fault (Zagros, Iran)", *Geophys. J. Int.*, **166**, 186- 196.

23. Yamini-Fard, F., Hatzfeld, D., Paul., A., Farahbod A.M., and Mokhtari, M. (2007). "The Diffuse Transition between the Zagros Continental Zone and the Makran Oceanic Subduction (Iran): Microearthquake Seismicity and Crustal Structure", *Geophys. J. Int.*, **170**, 182-194.

24. Zhu, L. (2000). "Crustal Structure Across the San Andreas Fault, Southern California, from Teleseismic Receiver Functions", *J. Geophys. Res.*, **105** (B2), 2969-2980.